Check for updates

Received: 12 October 2021 | Revised: 21 February 2022 | Accepted: 24 February 2022

DOI: 10.1111/ffe.13687

SPECIAL ISSUE ARTICLE

FFEMS Fatigue & Fracture of Engineering Materials & Structures WILEY

Corrosion fatigue and damage tolerance in the nickel-based superalloy RR1000 subjected to SO_2 environments

Martin Bache[1] | **Christopher Ball**[1] | **Mark Hardy**[2] | **Paul Mignanelli**[2]

[1]Institute of Structural Materials, Faculty of Science and Engineering, Bay Campus, Swansea University, Swansea, UK

[2]Rolls-Royce plc, Derby, UK

Correspondence
Martin Bache, Institute of Structural Materials, Faculty of Science and Engineering, Bay Campus, Swansea University, Swansea SA1 8EN, UK.
Email: m.r.bache@swansea.ac.uk

Funding information
Engineering and Physical Sciences Research Council (EPSRC), Grant/Award Numbers: EP/H022309/1, EP/H500383/1

Abstract

When exposed to a high-temperature corrosive environment, nickel-based superalloys may experience surface pitting and sulphide diffusion, which will influence concurrent or subsequent fatigue behavior. Sulphur, pre-existing in the environment or as a bi-product of burning fossil fuels, reacts with sodium (as an atmospheric pollutant), creating molten sodium sulphate deposits on the metal surface. Combined with sodium chloride, these deposits attack the protective oxide layer allowing sulphides to migrate along grain boundaries. Continued sulphide diffusion promotes a weakened subsurface layer, inducing grain dropout and fatigue crack initiation. The present investigation focussed upon the subsequent effects of exposure to SO_2 containing atmospheres on low cycle fatigue performance, together with the impact of an intermediate cleaning process. Damage tolerance data suggest that exposure to a SO_2 environment fails to affect fatigue crack growth threshold or Stage II growth behaviors when compared with standard laboratory air.

KEYWORDS

damage tolerance, fatigue, hot corrosion, nickel superalloy, pitting

1 | INTRODUCTION

Nickel-based superalloys are a natural choice for engineering applications that demand structural integrity at temperatures exceeding 600°C.[1] Despite their relatively high density, a resistance to oxidation and corrosion coupled with high static strength, creep tolerance, and fatigue endurance has sustained long-term employment in the high-pressure compressor and turbine sections of gas turbine aeroengines. To enable gains in fuel efficiency and to reduce emissions, the operating temperatures experienced by key components within the gas turbine are progressively increasing, to the point where hitherto benign combinations of temperature and gaseous environment may now introduce the potential for additional damage mechanisms.

Type II hot corrosion, resulting from the chemical reaction between the substrate alloy and molten eutectic salt deposits and usually prevalent across the temperature range 600–750°C, is one such mechanism that must now be considered.[2] Following dissolution and subsequent penetration of the protective oxide scale, itself composed

This is an open access article under the terms of the Creative Commons Attribution License, which permits use, distribution and reproduction in any medium, provided the original work is properly cited.
© 2022 The Authors. *Fatigue & Fracture of Engineering Materials & Structures* published by John Wiley & Sons Ltd.

of two distinct layers enriched in nickel/cobalt and titanium/chromium/aluminium, respectively, the molten salt deposits may penetrate the alloy surface and enhanced sulphur activity in this subsurface region gives rise to the precipitation of a continuous sulphide layer.

Specific to in-service, polycrystalline nickel components under hot corrosion fatigue conditions, examples have been reported where chromium- and titanium-rich sulphide particles have precipitated at subsurface grain boundaries in preference to forming the continuous sulphur-rich zone.[3,4] Future superalloy developments, required to resist such Type II damage, must incorporate an accurate assessment of fatigue behavior under representative operating conditions.[5] This is extremely challenging in the laboratory setting; however, previous papers have reported the design of in situ environment test cells for the assessment of structural metals under hot sulphur-bearing environments.[6]

From the perspective of mechanical behavior and fatigue in particular, hot corrosion may be especially problematic should the corrosive attack lead to the development of localized surface pits. Recent studies have evaluated the fatigue strength of alternative nickel superalloys subjected to pre-existing pitting damage,[7,8] and this supports the ranking of alloys based on environmental resistance. However, there remains a fundamental requirement to understand the role of cyclic stress on pit formation, the stress raising effect of corrosion pits, and the influence of hot corrosive environments on fatigue crack initiation and subsequent crack growth.

In the example of compressor or turbine rotor components, the precise form and location for hot corrosion pitting may be controlled by various factors. These include pre-existing geometric features, surface treatments, inherent gas composition, surface contaminants (e.g., ingested salts), and the substrate microstructure. To simulate these service conditions, specialist test equipment and procedures have been designed for the assessment of laboratory scaled test coupons.[9] Such systems need to address the surface preparation of specimens, pre-salting, prolonged isothermal heating, and mechanical loading under low and high cycle fatigue waveforms. Specific experiments may be conducted to characterize fatigue strength or fatigue crack growth to partition initiation and damage-tolerant behavior under hot corrosion environments.

In this study, fatigue strength was measured from plain cylindrical, shot peened specimens exposed to a SO_2 gas environment at 700°C to provide a "baseline" SN curve. Under these circumstances, the corrosion damage was accumulating concurrent with cyclic loading. This performance was then compared with specimens with pre-corroded pitting, either with the surface corrosion products fully retained or after a cleaning operation. Indeed, the response to various cleaning reagents and procedures formed a wider ranging objective of the present study.

All the scenarios described here are relevant to the design, operation, and lifing of critical rotating engine components. The experimental study was defined to support existing damage-tolerant component lifing methods. Recognizing that the total fatigue life measured in the low cycle fatigue (LCF) experiments represents a combination of initiation life and crack propagation, data from "long" crack growth testing will be presented to help partition the relevant importance of these different stages of damage and any unique consequences of crack growth under a hot corrosion environment. These include characterization of Stage II "Paris" crack growth together with an assessment of fatigue crack growth threshold behavior.

It is recognized that the transition from a corrosion pit to a true fatigue crack is highly complex, incorporating the effects of "small" and "short" scale growth during the early stages of crack development. Previous authors have monitored and evaluated the behavior of environmentally assisted short crack growth behavior in alternative alloys and in relatively benign aqueous environments at ambient temperatures.[10,11] However, the current investigation of high-temperature corrosion fatigue behavior was not intended to enable such characterization.

2 | EXPERIMENTAL METHODS

The current investigation focussed on the nickel-based superalloy RR1000 in fine-grained microstructural form. Plain cylindrical and corner crack test specimens were machined from a RR1000 forging. Proprietary thermomechanical processing and heat treatment had generated a standard fine-grained microstructure with an average grain size of 8 μm plus trimodal distribution of γ' strengthening particles (i.e., coarse primary γ' particles decorating the grain boundaries, with finer scale secondary γ' and tertiary γ' precipitates evenly distributed inside the grains). The grain size was measured using a standard line intercept method applied to multiple two-dimensional (2D) digital images (ASTM E112-10). The typical γ/γ' microstructure is illustrated in Figure 1; however, much greater detail on RR1000 thermomechanical processing and microstructural evolution, including resolution of the secondary and tertiary γ' particles, has been previously published by Mitchell et al.[12]

The plain cylindrical LCF specimens contained a 12 mm gauge length and 4.5 mm diameter. All specimens

were subjected to a shot peening operation using steel ball media across the entire, central gauge section. Shot peening conditions were selected to replicate the surface condition of relevant engine components; therefore, the precise control parameters are considered proprietary.

Isothermal, load controlled fatigue experiments were conducted at 700°C employing a triangular waveform at R = -1 and 0.17 Hz frequency (i.e., 6-s cycle period) with specimens cycled to complete rupture, that is, no run-outs are reported. Applied stress values were selected to generate failures over the range 10^3 to 10^5 cycles. All fatigue tests were performed within an environmental chamber under a flow of SO_2 gas (air + 300 ppm SO_2 at 80 ml/min).

The "baseline" response of the alloy was measured in the SO_2 gas environment utilizing as received, plain cylindrical, peened specimens (it is emphasized that these specimens were not subjected to prior corrosion of any form).

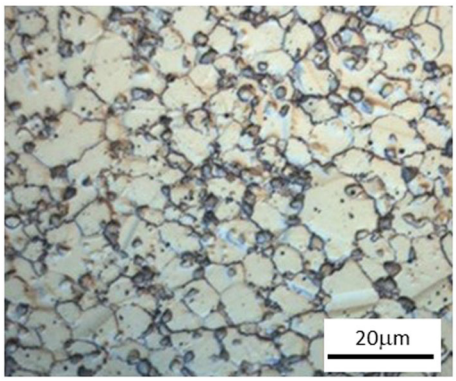

FIGURE 1 Fine-grained microstructure in RR1000. Near-equi-axed γ grains (light regions) with γ′ particles decorating the grain boundaries [Colour figure can be viewed at wileyonlinelibrary.com]

Alternatively, additional specimens were subjected to hot corrosion under zero applied stress prior to fatigue testing. All classes of "pre-corroded" specimen were initially heated to 100°C and sprayed with a sodium chloride salt solution (98% Na_2SO_4 + 2% NaCl dissolved in 45-ml methanol and 55 ml of water), resulting in a salt flux of 0.15 mg/cm^2. The typical appearance of such salted specimens after returning to room temperature is illustrated in Figure 2. Different hot corrosion sequences were then applied to selected salted specimens to provide the three classifications of specimen described in Table 1.

Pre-corroded specimens were cooled to room temperature between each stage of exposure. "Cleaning" refers to a soak in Ardrox© 1435 solution (30% concentration) for 4 h at room temperature followed by a rinse with flowing distilled water. In all cases, the calculation of the load required to achieve an applied test stress was based on non-contacting measurements of the gauge diameter, after shot peening and prior to salting and/or corrosion.

Post-LCF fatigue testing, specimen fracture surfaces plus the gauge surface were inspected using optical and scanning electron microscopes, with particular attention given to the identification of the critical crack initiation site and any secondary cracking on the exposed fracture plane. Chemical species incorporated within the corrosion products, either distributed across the gauge surface or localized in the vicinity of relevant corrosion pits, were identified using energy-dispersive X-ray spectroscopy (EDS).

FIGURE 2 Example of a shot peened and salted LCF specimen prior to fatigue testing [Colour figure can be viewed at wileyonlinelibrary.com]

TABLE 1 Pre-corrosion scenarios

Designation	1st exposure	Cleaned	2nd exposure
SNS	700°C for 200 h in 300 ppm SO_2	No	700°C for 200 h in 300 ppm SO_2
SYS	700°C for 200 h in 300 ppm SO_2	Yes	700°C for 200 h in 300 ppm SO_2
SYA	700°C for 200 h in 300 ppm SO_2	Yes	700°C for 200 h in air

Fatigue crack growth measurements, conducted to ASTM E647, employed 7 × 7 mm square section specimens containing a starter slit machined by a diamond wheel at the mid length position along one edge. The growth of the part through quarter circular crack was monitored using a pulsed DC potential drop monitoring system. Full background on the corner crack test technique, DCPD calibrations, and associated stress analysis can be found in previous publications.[13,14] Largely influenced by the resolution of the digital voltmeter utilized for DCPD monitoring, instantaneous crack length was measured to an accuracy of 3 μm.

Stage II Paris crack growth was measured using relatively fast "cyclic" waveforms (i.e., 5-Hz sine and 15 cycles per minute trapezoid). All corner crack propagation tests were performed under R = 0.1 at 700°C. Data are compared from as machined specimens tested under standard laboratory air and a hard vacuum (<10^{-5} mbar) condition. A set of specimens was also subjected to pretest salting and exposure to the same flow of SO_2 during crack growth as described for the LCF assessment. An example of a pre-salted specimen is illustrated in Figure 3. To avoid freely initiated cracking during the hot corrosion testing, the specimen was masked during the application of the salt spray excluding a 2-mm-wide region, which encompassed the starter slit and predicted plane of cracking.

The same corner crack geometry was employed for fatigue crack growth threshold testing. A constant K_{max}/increasing R ratio technique was selected utilizing a 5-Hz sine waveform. The precise ΔK_{th} values were established as per ASTM E647 at a growth rate of 10^{-10} m/cycle, although selected experiments continued to even slower growth rates. The constant K_{max} technique[15] was deliberately adopted to provide a lower bound measurement of ΔK_{th} (given the inverse relationship between threshold value and R ratio) utilizing a minimum number of available specimens. From the engineering perspective, this also presents a conservative approach.

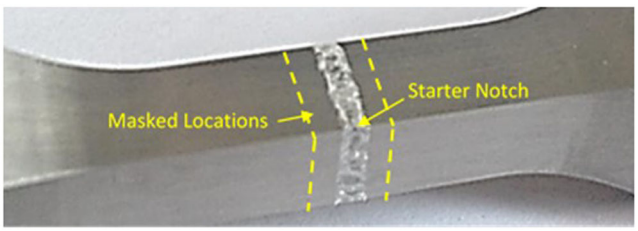

FIGURE 3 Pre-salted corner crack specimen employed for hot corrosion fatigue crack growth testing in a SO_2 gas environment [Colour figure can be viewed at wileyonlinelibrary.com]

3 | RESULTS

The LCF response of peened and salted specimens tested at 700°C in the SO_2 gas environment is plotted in Figure 4. A best fit trend line has been superimposed through this "baseline" dataset to help compare to the relative performance of pre-corroded specimens. The baseline data span lives of 10^4 to 10^5 cycles.

Compared with the baseline response, all pre-corroded specimens demonstrated a reduction in fatigue life irrespective of corrosion scenario. This can be considered either in terms of "life to first crack" or "safe stress" design and component lifing philosophies. In the first instance, for a given applied stress condition, the life of pre-corroded specimens is reduced by approximately one order of magnitude. For the latter, a reduction in stress of approximately 150 MPa induced an equivalent life to the baseline data. These relative shifts in performance are emphasized by the two schematic arrows superimposed on the SN graph.

The number of individual specimens available to define the SN curves for either dataset was limited. A degree of scatter was highlighted among the combined pre-corroded specimen data, noting that the classical inverse relationship between applied stress and cyclic life was not consistent. It appears that pre-corroded specimens performed in a similar manner irrespective of cleaning between the exposure treatments and whether the exposures incorporated a SO_2 or air environment.

Inspection of the specimen fracture surfaces indicated that all specimens initiated multiple cracks from distributed surface corrosion pits. The example from a baseline specimen in Figure 5 illustrates that limited crack growth occurred from numerous individual shallow pits around the periphery of the gauge section, now exposed as a lustrous outer ring. Ultimately, crack growth dominated from a single pit (arrowed) on a distinct plane, forming a regular, elliptical final fatigue crack profile. The example from a pre-corroded specimen in the same figure displays an almost identical region of tensile overload to the baseline specimen. However, more extensive fracture has progressed from at least 10 pits distributed around the lower portion of the gauge circumference, with adjacent cracks on slightly different planes coalescing, forming steps on the fracture surface and an irregular final fatigue crack profile. This difference in pit to crack transition behavior was consistent for all baseline specimens compared with their pre-corroded counterparts. Notably, the two specimens illustrated in Figure 5 were tested at an identical stress condition (σ_{max} = 650 MPa). Significantly different fatigue lives were measured for these specimens, with the baseline specimen failing after N_f = 63,271 compared with N_f = 2,168 for the pre-corroded equivalent.

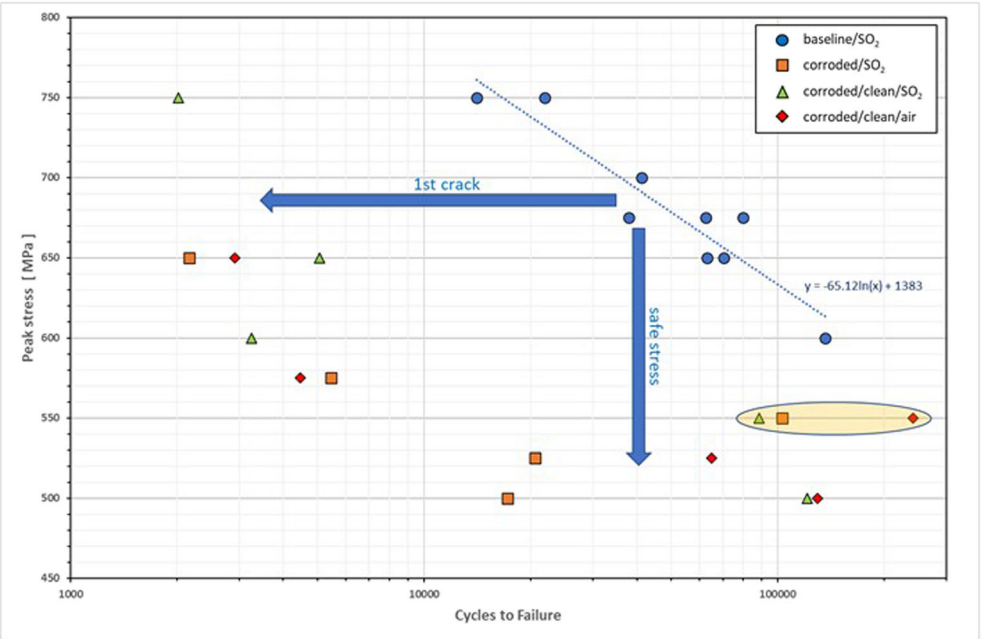

FIGURE 4 Low cycle fatigue behavior [Colour figure can be viewed at wileyonlinelibrary.com]

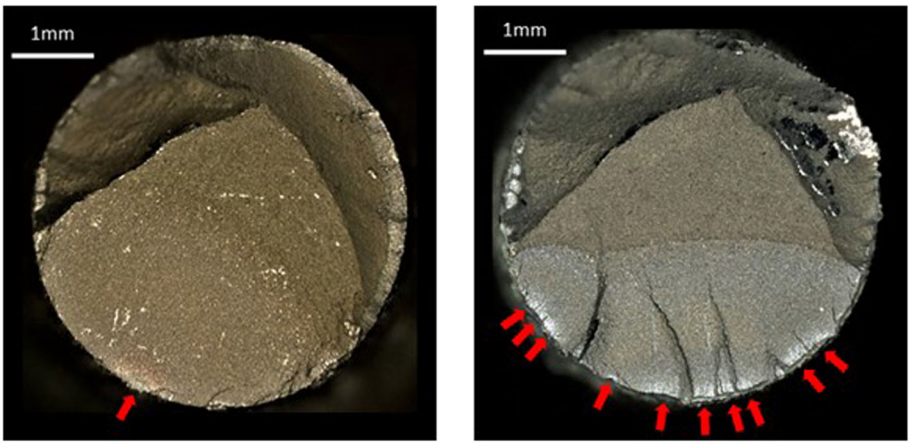

FIGURE 5 Typical fracture surfaces generated in (left) baseline specimen, $\sigma = 650$ MPa, $N_f = 63{,}271$ and (right) pre-corroded specimen ($\sigma = 650$ MPa, $N_f = 2{,}168$). Both tested in the SO_2 gas environment [Colour figure can be viewed at wileyonlinelibrary.com]

The detailed form and metrics of corrosion pits were best defined from the various cleaned specimens where surface corrosion product had largely been removed (Figure 6). When performing EDS inspections of such pits, at least on this scale of magnification and directly from the fracture surface, it was pertinent to note the even distribution of remnant sulphur and a lack of concentration of this element around the base of the pit, in contrast to an apparent concentration of cobalt and nickel. The earliest stages of cracking appeared slightly facetted before a gradual transition to transgranular fracture.

Selected specimens were also subjected to sectioning on a plane parallel to the longitudinal test piece axis to intersect corrosion pits and expose the subsurface microstructure and chemical distribution (Figure 7). This specific example illustrates a relatively wide pit (i.e., depth to width ratio a/c ~3). However, the pit profiles were highly variable (ranging between $\infty \leq a/c \leq 1$) and sensitive to the precise local microstructure and grain dropout. Cracking selectively focussed on sites of surface breaking grain boundaries exposed around the pit periphery. These boundaries, orientated near orthogonal to the tensile stress axis, promoted the ingress of SO_2 under the application of cyclic stress. These polished sections at higher magnification helped to identify the presence of grain boundary sulphides below the base of the pits. It was also common for such sectioning to reveal multiple secondary cracks emanating from the pit periphery. However, sulphides were not detected along the extended crack wake.

Stage II fatigue crack growth data measured at 700°C are presented in Figure 8. Comparing the data under hard vacuum to tests performed in oxidizing environments (air or SO_2) demonstrates a fundamental increase

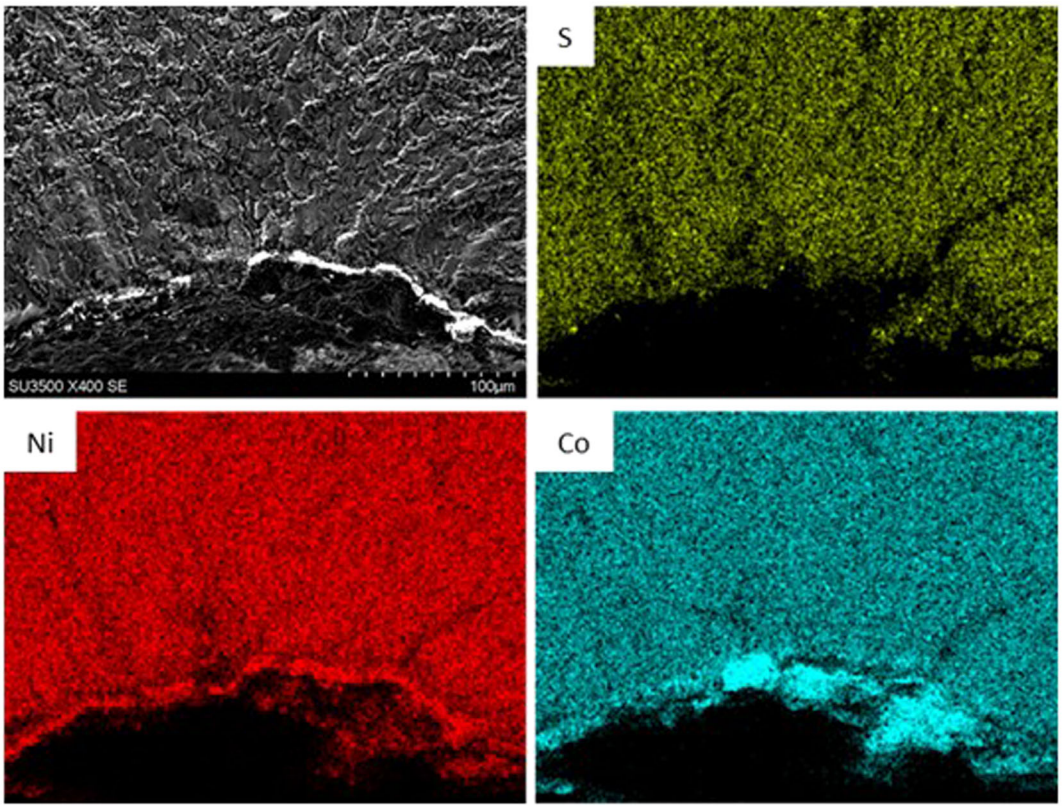

FIGURE 6 Fractography of crack initiation from a corrosion pit (top left) and corresponding EDS maps for sulphur, nickel, and cobalt (from a pre-corroded SYS specimen) [Colour figure can be viewed at wileyonlinelibrary.com]

in growth rates through the presence of oxygen, but notably, no accelerated growth was detected in the hot corrosion SO_2 environment.

Near-threshold fatigue crack growth data measured at 700°C are presented in Figure 9. Compared with three tests performed in air at various constant K_{max} conditions, the result from the test performed on a pre-salted specimen in SO_2 gas essentially demonstrated identical behavior. The ΔK_{th} values defined from these tests as calculated to ASTM E647 are listed in Table 2.

4 | DISCUSSION

During the present matrix of LCF testing, the strongest fatigue response was clearly demonstrated by the previously un-corroded "baseline" specimens tested in the SO_2 gas environment. Under this scenario (i.e., salting alone then followed by fatigue), the total measured fatigue life would be a summation of initiation and propagation cyclic lives relevant to the dominant crack that eventually led to failure.

$$N_{tot} = N_i + N_{FCG} \tag{1}$$

where in this case the term N_i refers to the number of cycles required to initiate a "crack-like discontinuity" emanating from the in situ corrosion damage across the gauge surface. The term N_{FCG} would represent the number of cycles for this crack to reach instability under cyclic loading and then induce tensile overload.

Under the present hot corrosion fatigue scenario and experimental setup, although a model invoking "small," "short," and "long" crack growth can be envisaged,[10] the characterization of the earliest stages of crack development was limited to post-test fractography and metallographic sectioning. It was impossible to partition cyclic lifetimes apportioned to "initiation" and "growth" with precise accuracy, and indeed, this was not a prerequisite of the study.

It was interesting to note that crack growth and eventual failure were typically concentrated from a single pit in the baseline specimens. Therefore, although multiple pits may have initiated small cracks, it was the first of these to exceed the long crack growth threshold

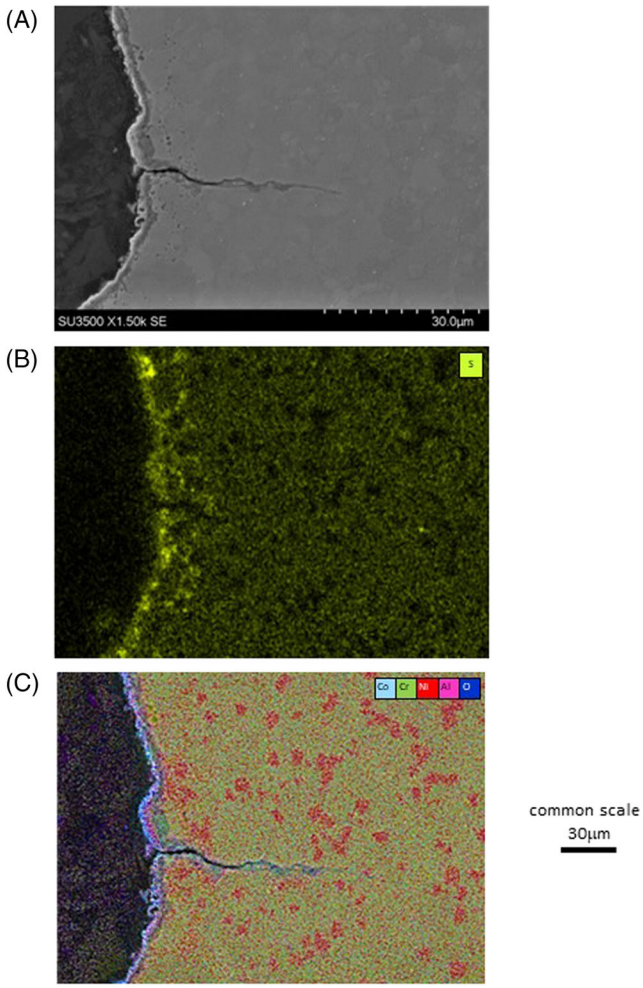

FIGURE 7 (A) Metallographic section through a corrosion pit with secondary cracking (from a pre-corroded SYS specimen); (B) EDS map of subsurface sulphides; (C) EDS map of oxidation associated with the crack wake [Colour figure can be viewed at wileyonlinelibrary.com]

condition, which then became dominant and produced the fatigue failure. A more recent investigation[16] employing an alternative nickel-based superalloy but under identical experimental procedures has helped develop a greater statistical understanding of this phenomenon. Interrupted "baseline" tests were subjected to longitudinal sectioning and polished to reveal a series of corrosion pits along the opposing edges of the specimen gauge section. Multiple pits, in the order of hundreds under certain stress/life conditions, illustrated small intergranular cracks initiating from their base and extending to a few tens of microns below the receding gauge surface. This indicates that under extreme hot corrosion fatigue conditions, the population of freely initiating cracks could be significant, and from an engineering perspective, it is important to ensure that such cracks remain non-propagating. Knowledge of the fatigue crack growth threshold characteristics was therefore an essential outcome from the present study.

That same exercise also accentuated the philosophical argument concerning the retrospective definition of the projected length of any surface crack. The continual process of surface recession and the disappearance of the original metal/atmosphere interface acting as a measurement reference, progressive thickening of the corrosion scale, and whether this scale acts as an effective load-bearing element all have implications for crack size measurements. The highly complex interaction between the chemical processes active at the surface and the time-dependent nature of the fatigue cycle has also been considered by a concurrent study.[17] The component lifing philosophies offered by Chan et al essentially concur with the present research while reiterating that the description of pit to crack transition illustrated in Figure 10 may be

FIGURE 8 Stage II "Paris" fatigue crack growth data measured in vacuum, air, and SO_2 gas environments at 700°C [Colour figure can be viewed at wileyonlinelibrary.com]

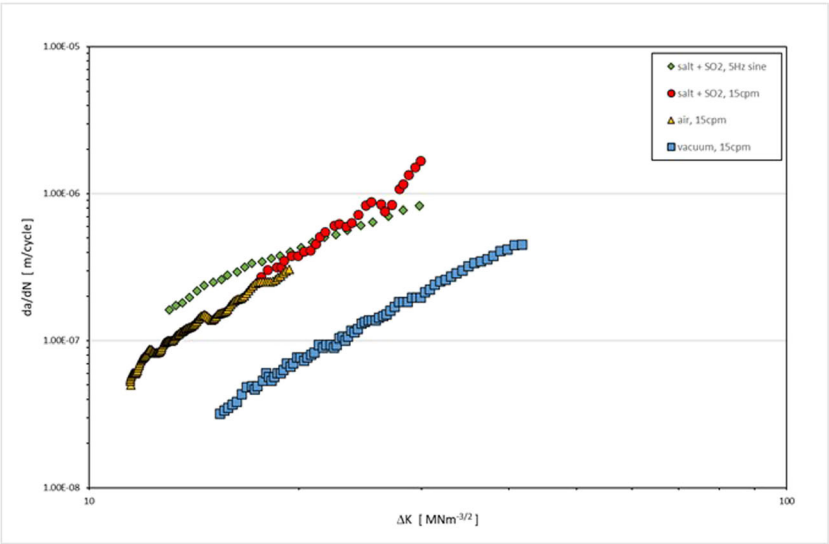

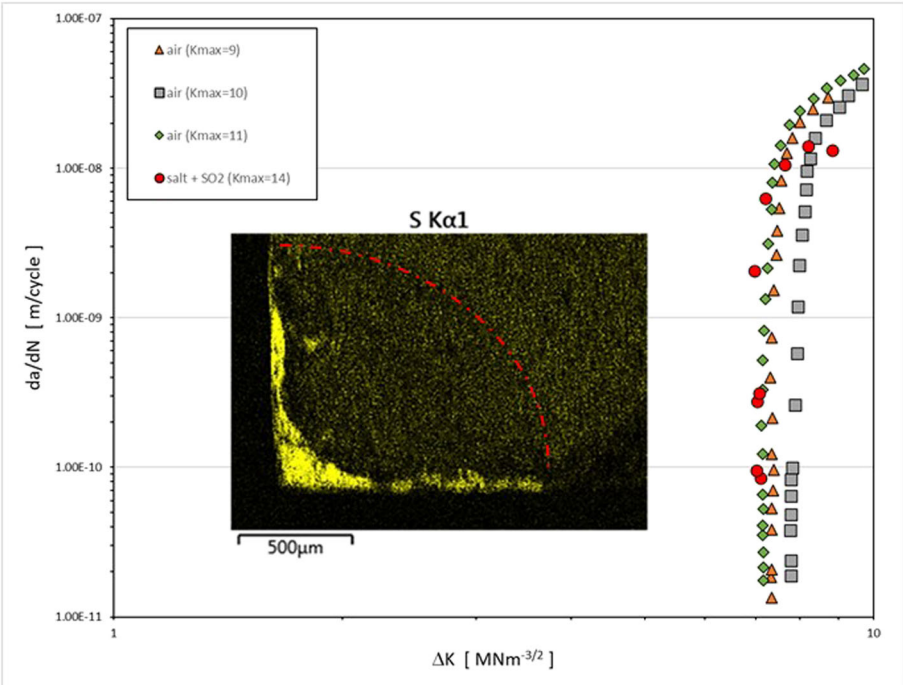

FIGURE 9 Fatigue crack growth threshold data for corner crack specimens tested in air and SO_2 gas at 700°C [Colour figure can be viewed at wileyonlinelibrary.com]

TABLE 2 Fatigue crack growth threshold values

Environment and K_{max} ($MNm^{-3/2}$)	R ratio at crack arrest	ΔK_{th} ($MNm^{-3/2}$)
Air (11)	0.47	7.10
Air (10)	0.52	7.82
Air (9)	0.51	7.42
Salt + SO_2 (14)	0.56	6.99

idealistic. They predicted that under representative conditions, nickel-based turbine discs will initiate corrosion pits very early into service, followed by an extensive period of transition prior to "long crack" extension to failure. Similar to the present research, the full complexity of the corrosion fatigue scenario could not be addressed under that study, for example, multiple pit/crack development and coalescence was not modeled, and it was proposed that the hot corrosion process would not be pertinent at all stages throughout the flight cycle.

Undoubtedly, cyclic plasticity and the superposition effects of surface residual stresses due to shot peening would have influenced the crack initiation and early growth mechanisms relating to the present tests.[18,19] However, the residual surface compressive stress (proprietary information) was deliberately kept constant throughout the course of the experimental matrix to provide a focus on the role of the environment and cleaning operations in controlling the chemical reaction at the interface between the metal substrate, surrounding SO_2 environment, and molten salt. The fundamental hot corrosion mechanism describing the high-temperature reaction of nickel to sulphur-bearing environments under static load has been described in much detail[20] and more recently considered under fatigue scenarios.[21] Essentially, the formation of a continuous oxide scale, as would be expected under standard laboratory air conditions, is disrupted by the ingress of sulphur into the surface layers of the substrate. Where this occurs preferentially along grain boundaries, a "necklace" structure of sulphides may form and with continued mechanical cycling surface grains can drop out to form an embryonic corrosion pit. The synchronous effects of grain boundary embrittlement and localized geometric stress concentration can subsequently encourage fatigue crack initiation from the base of the pit, especially at sites where the sulphidation forms as a V-shaped protrusion between grain boundaries. The irregular profiles at the base of the corrosion pits generated during the present study were consistent with this intergranular sulphide and grain dropout model, as evidenced by the metallographic section through a single pit in Figure 11. This fracture mode contrasts with classical fatigue models invoking intrusion/extrusion formation and an immediate transition to transgranular growth.[22] Due to the complexity and scale of this mechanism, from an empirical perspective, the transition from corrosion pitting to crack growth will always be extremely difficult to detect in practice. Previous workers[10,11] have been able to quantify small crack growth rates from cracks emanating from pre-existing

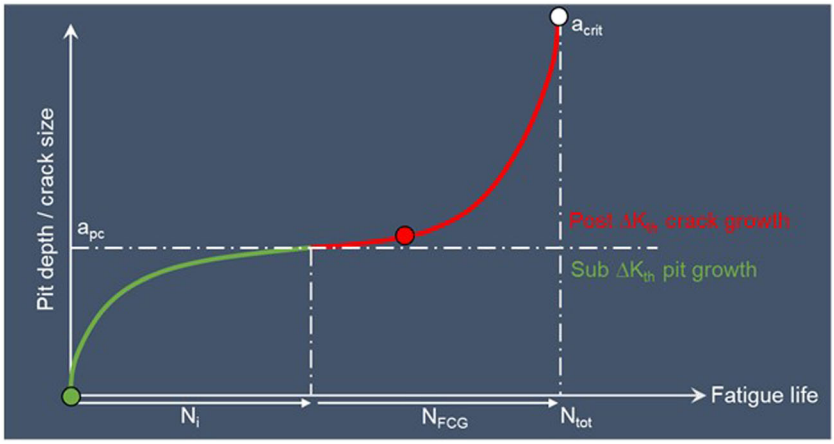

FIGURE 10 Schematic model to define sub and post threshold corrosion pit to crack transition nomenclature [Colour figure can be viewed at wileyonlinelibrary.com]

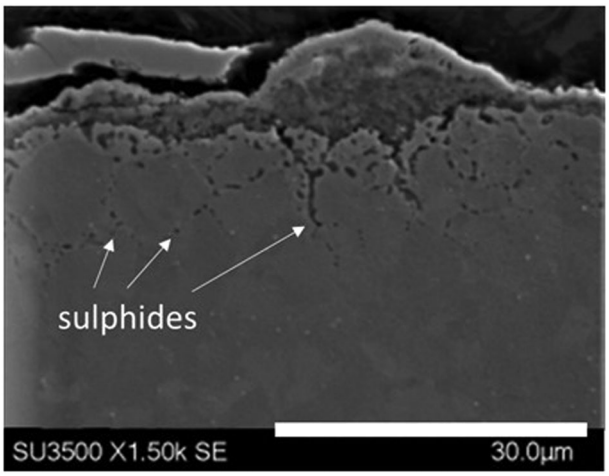

FIGURE 11 Intergranular sulphides decorating grain boundaries and responsible for progressive surface grain dropout

corrosion pits, notably under aqueous corrosion scenarios at ambient temperatures. This was an impossible task for the freely initiating cracks developed in the current plain cylindrical specimens at high temperature. However, it is probable that the formation of sulphides on the subsurface grain boundaries influenced early crack growth rates.

In the baseline, previously un-corroded specimens, pitting was prevalent across the entire gauge section surface and multiple, physically short, subcritical cracks (i.e., $a_{pc} \leq a \leq a_{crit}$) initiated at many distributed sites. However, once exceeding the critical defect size inherent to the fatigue crack growth threshold value (ΔK_{th}), a single crack eventually dominated and progressed to ultimate failure (Figure 5). This "subthreshold," pitting-dominated behavior is illustrated schematically in Figure 10. In contrast, all pre-corroded specimens entered into long crack behavior from multiple pits immediately on cyclic loading.

The potential for sulphide ingress would be continuous throughout the entire course of all tests performed in the SO_2 gas atmosphere. However, sulphides were never detected along the wake of the developing "long" crack. Instead, sulphides were constrained to the gauge surface regions and very early flanks of the crack, typically within a depth of 20 μm of the base of the pit (effectively two to three grain diameters). Therefore, it is considered that the rate of long crack growth exceeded the competing migration of environmental sulphur. In any case, the Stage II crack measurements in Figure 8 support the argument that the ingress of SO_2 gas would not affect the rate of growth of the crack, not at least above the effects of oxidation, once advancing from the corrosion pit and beyond the surface layer of grain boundary sulfide decoration.

Multiple crack initiation was also prevalent among all classes of pre-corroded specimens, irrespective of cleaning between the static hot corrosion and fatigue testing phases. However, crack growth initiated from a greater number of individual pits in the corroded specimens, with eventual failure occurring through the coalescence of adjacent cracks on a common plane (Figure 5). It appears that under the preliminary static corrosion treatment, a significant number of pits had exceeded the critical defect size ($a > a_{pc}$) such that many sites supported local crack growth once fatigue loading commenced. It is pertinent that the combined 400 h spent under static corrosion exceeded the test duration experienced by any of the baseline test specimens while exposed to cyclic stress and SO_2 gas. Once again, crack initiation was intimately related to intergranular sulphide embrittlement at the base of the pits (Figure 7A), but with no further ingress of sulphur associated with the developing long crack (Figure 7B). In contrast, oxidation was detected along the entire length of the crack flanks via EDS and optical imaging (Figure 7C). The predominant transgranular, long crack fracture mode detected

here compared favorably to many previous investigations of "fast cycle" crack growth in various microstructural forms of this alloy in the same temperature range.[23]

Referring again to Figure 10, all pre-corroded LCF specimens would be associated with "post-threshold" behavior. It is reasonable to assume that the pre-existing pitting minimized or even eliminated the initiation life of the pre-corroded specimens, with "long" crack growth encouraged from the very earliest loading cycles, effectively bypassing any short crack phenomena proposed to describe corrosion fatigue mechanisms.[24] Schematically, the scale of any pre-existing defect is represented by an arbitrary point superimposed on the growth curve in Figure 10.

Measurements were taken of the pits identified at the initiation sites of every pre-corroded specimen (those that ultimately led to macroscopic failure), and these ranged from a minimum of 45 μm in depth to a maximum of 95 μm. Considering the scenario that represents the lower bound in crack growth performance,

i. the fatigue crack growth threshold value ($\Delta K_{th} = 6.99 MNm^{-3/2}$) obtained for salt-laden RR1000 specimens in SO_2 gas (see Figure 9 and Table 2),
ii. the lowest applied stress condition employed across the test matrix ($\sigma_{max} = 500$ MPa at $R = -1$), and
iii. the minimum pit metric (i.e., depth = 45 μm)

these relevant parameters were integrated into an AFGROW model[25] to simulate a semielliptical 2D surface flaw subjected to cyclic loading in a cylindrical cross-sectional specimen. Immediate crack growth was predicted.

In fact, AFGROW calculations invariably predicted crack growth would commence from the very first load cycle for all combinations of pit depth and applied stress employed during the current test matrix on pre-corroded specimens. This exercise may be considered simplistic, not least for representing a complex pit geometry by a simple 2D discontinuity and solely employing the lower bound constant K_{max} threshold value. However, within the context of the present study, we suggest this represents a rational engineering approach and the consistent threshold behavior measured in air and SO_2 was also encouraging to note.

Significantly, there was no direct relationship between the measured pit depths and the associated LCF lives to failure. This was not unexpected, because from a fatigue perspective, the local stress raising effect of the corrosion pit must be controlled by a combination of factors and not simply the depth (e.g., pit depth, surface opening, precise peripheral geometry, and interactions with local sub-pit microstructural features must also be considered).[26]

It should be emphasized that no consideration was given to the effects of shot peening on the stress intensity driving force during the damage tolerance modeling. Concurrent studies are, however, characterizing the complex interactions between hot corrosion pitting, surface roughness, residual stress, and work hardening. It is worthwhile reiterating that despite shot peening being applied to all of the current LCF test specimens, no evidence of subsurface crack initiation was ever detected, emphasizing the critical role of the hot corrosion damage. The same general oxidation/sulphidation, corrosion pitting, and grain dropout behavior have also been noted during subsequent studies utilizing unpeened, polished specimens.

Three anomalous data points are highlighted in Figure 4. These relate to three separate tests performed at a common normalized stress level of 550 MPa, where a relatively strong response was measured compared with the general SN curve for the combined pre-corroded specimen datasets. A common feature was noted during inspection of these three specimens prior to fatigue loading. The gauge sections had retained a continuous protective oxide layer across the surface, thus protecting the substrate from sulphide attack and corrosion pitting. An example is illustrated in Figure 12 and compared with the typical surface appearance displayed by the majority of corroded samples. The precise reason for such variation in corrosion response is unknown, particularly as the fatigue specimens were pre-corroded in batches, not

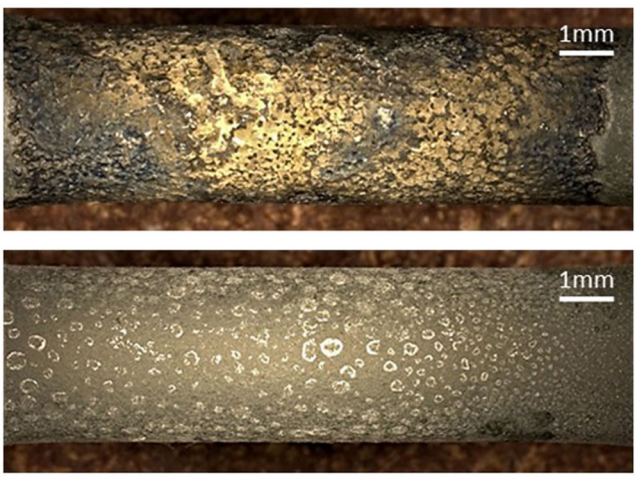

FIGURE 12 Variable hot corrosion response demonstrated in two specimens prior to LCF testing, both subjected to the SYS pre-corrosion scenario. (Top) Corrosion pitting exposed due to the spallation of surface oxide scale (typical of most specimens). (Bottom) Continuous oxide scale retained and lack of pitting [Colour figure can be viewed at wileyonlinelibrary.com]

individually. It is impossible to provide a definitive retrospective explanation but factors that could be responsible include differences in machining process, shot peening anomalies, surface residual stress state, specimen handling, variance of salting concentration/distribution, or any combination of these parameters. Whatever the reason, the absence of stress raising corrosion pits naturally appeared to improve fatigue strength.

From a damage tolerance lifing perspective, it was reassuring to note that neither crack growth threshold nor "long" crack growth behavior was affected by a hot corrosion SO_2 environment. Inspection of the pre-salted corner crack threshold specimen tested in SO_2 demonstrated that salt contamination on the gauge surface generated sulphide deposits along the flanks of the crack. This is illustrated by the fracture surface image superimposed on Figure 9 incorporating EDS mapping. These features were most prevalent on this sample because of the prolonged period of exposure during the threshold test procedure. It is impossible to conclude whether these sulphides formed concurrent with the crack advancing or developed behind the crack tip in the wake of cracking. A previous study employed advanced atom probe characterization techniques to identify sulphide reactions at subsidiary crack tips in specimens sourced from this same research project.[27] Notably, those samples related to identical corner cracks growing in a salt and SO_2 environment were characterized on a near-surface plane. Irrespective of the precise crack tip damage mechanism, no significant effect on the rate of crack growth was reported because of the complex sulphidation reactions, and those findings are replicated by the current data.

Figure 9 also demonstrates the absence of sulphides "wicking" into the part through quarter circular crack interior. The depth of the sulphide regions appear to be time dependent, being greatest immediately adjacent to the starter slit/specimen edge and tapering down toward the crack front. The presence of surface salt deposits appears to be intrinsic to sulphide formation. The SO_2 gaseous environment undoubtedly penetrated across the entire fracture surface and was thereby active around the entire crack front. This gas infiltration would have been promoted by the constant K_{max} threshold technique, effectively maintaining the crack fully open throughout fatigue cycling. Also, a slightly increased value of K_{max} was deliberately employed for the SO_2 test, relative to the equivalent air tests, to further encourage crack opening. Despite this potential for environmentally assisted crack growth, the quarter circular profile was retained during the experiment (the approximate crack front position is marked in Figure 9), and the generic transgranular crack mode was unaffected. The oxide tinted crack surfaces and measured growth rates were consistent with tests performed in standard laboratory air at the same temperature.

In service, salts may be ingested into the gas turbine engine from the atmosphere during flight, especially from low-altitude operations over sea water, but also during taxi operations on the ground. Compounds of sulphur are generated during the combustion of aerospace-grade kerosene. The composition of the salting solution, the salt density generated by the spray application, and the elevated test temperature employed during the present study are, in combination with cyclic stressing, thought to provide a reasonable laboratory simulation of the conditions experienced by compressor and turbine rotor components during gas turbine operations. In addition, the assessment of selected specimens that had incorporated a cleaning procedure is relevant to standard off-wing inspection routines applied throughout the life of disc components. The potential effects of cleaning on fatigue performance were a major driver behind the present study. It was encouraging, therefore, to note that the addition of a simulated cleaning process failed to induce any adverse effect on fatigue strength. As the basis for fatigue characterization, the capability to perform testing under a hot corrosion environment is more representative than traditional testing in laboratory air. The present study has, therefore, provided valuable data for the fundamental understanding of nickel-based superalloys exposed to such aggressive working environments and will support future component design and lifing methods.

5 | CONCLUSIONS

The following high-level conclusions were drawn from the present study:

i. Specific to the combined salt and gas compositions under investigation, hot corrosion led to the ingress of sulphur, formation of sulphides along grain boundaries, and grain dropout to form pits, both under static and fatigue loading conditions.
ii. Corrosion pits, whether pre-existing or forming concurrent with fatigue loading, controlled the initiation of fatigue cracks. Multiple cracks initiated in the individual specimens.
iii. Fatigue strength was reduced in specimens containing pre-existing corrosion pits and was insensitive to the precise combination of exposure environment and/or cleaning.
iv. Fatigue crack growth threshold and Stage II crack growth rates were not affected by a hot corrosion SO_2 environment.

ACKNOWLEDGMENTS

The research was funded by the Engineering and Physical Sciences Research Council (EPSRC) Rolls-Royce Strategic Partnership in Structural Metallic Systems for Gas Turbines (grants EP/H500383/1 and EP/H022309/1). The provision of materials and technical support from Rolls-Royce plc (Derby, UK) is gratefully acknowledged. Mechanical testing was performed at Swansea Materials Research & Testing (SMaRT) Ltd. Five of the baseline LCF tests were performed under a previous project but at the same laboratory by Dr. Hollie Cockings.

DATA AVAILABILITY STATEMENT

Data relating to the present submission are subject to commercial IP. Detailed access to the data will be considered, however, following written requests to the corresponding author (MRB) and consideration by Rolls-Royce plc.

NOMENCLATURE

ΔK	applied range of stress intensity
ΔK_{th}	minimum value of ΔK to sustain crack growth (threshold)
a	crack length
a_{crit}	critical crack length at fracture
a_{pc}	pit depth at transition to crack
AFGROW	crack propagation prediction software
da/dN	fatigue crack growth for a single load cycle
K_{max}	maximum applied stress intensity per cycle
EDS	energy-dispersive X-ray spectroscopy
LCF	low cycle fatigue
N_{FCG}	number of cycles under crack growth
N_i	number of cycles to initiation
N_{tot}	total number of cycles to failure
SN	stress versus cycles
SO_2	sulphur dioxide (gas)

ORCID

Martin Bache https://orcid.org/0000-0001-6932-7560

REFERENCES

1. Reed RC. *The Superalloys*. Cambridge University Press; 2006.
2. Goebel JA, Pettit FS, Goward WG. Mechanisms for the hot corrosion of nickel-base alloys. *Metall Trans*. 1973;4(1):261-278.
3. Viswanathan R. Investigation of blade failures in combustion turbines. *Eng Fail Anal*. 2001;8(5):493-511.
4. Whittle DP, Misra AK. Effects of SO2 and SO3 on the Na2SO4 induced corrosion of nickel. *Oxid Met*. 1984;22-1(1-2):1-32.
5. Child D, Meldrum J, Onwuarolu P. Corrosion-fatigue testing of Ni-based superalloy RR1000. *Mat Sci Tech*. 2017;33(9):1040-1047.
6. Rosier H, Perkins K, Girling A, Leggett J, Gibson G. Factors affecting the corrosion fatigue life in nickel based superalloys for disc applications. In: *EUROSUPERALLOYS 2014 – 2nd European Symposium on Superalloys and their Applications*: MATEC Web of Conference; 2014;14:03001.
7. Mahobia GS, Paulose N, Mannan SL, Sudhakar RG, Chattopadhyay K, Srinivas NCS. Effect of hot corrosion on low cycle fatigue behavior of superalloy IN718. *Int J Fatigue*. 2014;59:272-281.
8. Gabb TP, Telesman J, Hazel B, Mourer DP. The effects of hot corrosion pits on the fatigue resistance of a disk superalloy. *J Mater Eng Perform*. 2009;19-1(1):77-89.
9. Dowd M, Perkins KM, Child DJ. Pre-notched and corroded low cycle fatigue behaviour of a nickel based alloy for disc rotor applications. *Int J Fatigue*. 2017;105:7-15.
10. Turnbull A. Reflections on early stages of environmentally assisted cracking from corrosion pits. *Corros Mater Degrad*. 2021;2(4):568-581.
11. Burns JT, Larsen JM, Gangloff RP. The effect of initiation feature on microstructure-scale crack propagation in Al–Zn–Mg–Cu. *Int J Fatigue*. 2012;42:104-121.
12. Mitchell RJ, Lemsky JA, Ramanathan R, Li HY, Perkins KM, Connor LD. Process development and microstructure and mechanical property evaluation of a dual microstructure heat treated advanced nickel disc alloy. In: Reed RC, ed. *Proc. of Superalloys 2008*. The Minerals, Metals and Materials Society; 2008:347-356.
13. Mom AJA. Revised working document for the AGARD cooperative test programme on titanium alloy disc engine material, Appendix A. AGARD Engine Disc Cooperative Test Programme. AGARD-R-766. 1988.
14. Pickard AC. *The Application of 3-Dimensional Finite Element Methods to Fracture Mechanics and Fatigue Life Prediction*. Engineering Materials Advisory Services Ltd.; 1986.
15. Tesch A, Pippan R, Doker H. New testing procedure to determine da/dN–ΔK curves at different, constant R-values using one single specimen. *Int J of Fatigue*. 2007;29(7):1220-1228.
16. Private data. Rolls-Royce plc; 2021.
17. Chan KS, Enright NP, Moody JP, Fitch SHK. Physics-based modeling tools for predicting type II hot corrosion in nickel-based superalloys. In: Hardy M, Huron E, Glatzel U, et al., eds. *Proc. of Superalloys 2016*. The Minerals, Metals & Materials Society; 2016:917-925.
18. McMahon ME. Review of residual stress impingement methods to mitigate environmental fracture susceptibility. *Corrosion and Materials Degradation*. 2021;2(4):582-602.
19. Gibson GJ, Perkins KM, Gray S, Leggett AJ. Influence of shot peening on high-temperature corrosion and corrosion-fatigue of nickel based superalloy 720Li. *Mater High Temp*. 2016;33(3):225-233.
20. Gheno T, Gleeson B. On the hot corrosion of nickel at 700°C. *Oxidation of Metals*. 2015;84(5–6):567-584.
21. Cockings HL, Perkins KM, Dowd M. Influence of environmental factors on the corrosion-fatigue response of a nickel-based superalloy. *Mat Sci Tech*. 2017;33(9):1048-1055.
22. Suresh S. *Fatigue of Materials*. Cambridge University Press; 1991.
23. Li HY, Sun JF, Hardy MC, et al. Effects of microstructure on high temperature dwell fatigue crack growth in a coarse grain PM nickel based superalloy. *Acta Mater*. 2015;90:355-369.
24. Larrosa NO, Akid R, Ainsworth RA. Corrosion-fatigue: a review of damage tolerance models. *Int Mater Rev*. 2018;63(5):283-308.

25. AFGROW, version 4.11.14.0. 2006.
26. Crawford BR, Loader C, Ward AR, et al. The EIFS distribution for anodised and corroded 7010-T7651 under constant amplitude loading. *Fatigue Fract Eng Mater Struct*. 2005;28(9): 795-808.
27. Pedrazzini S, Child DJ, Aarholt T, et al. On the effect of environmental exposure on dwell fatigue performance of a fine-grained nickel-based superalloy. *Metall Mater Trans a*. 2018; 49(9):3908-3922.

How to cite this article: Bache M, Ball C, Hardy M, Mignanelli P. Corrosion fatigue and damage tolerance in the nickel-based superalloy RR1000 subjected to SO_2 environments. *Fatigue Fract Eng Mater Struct*. 2022;1-13. doi:10.1111/ffe.13687